Journal of Hazardous Materials 179 (2010) 692–700

Contents lists available at ScienceDirect

Journal of Hazardous Materials

journal homepage: www.elsevier.com/locate/jhazmat

# Effects of shape, porosity, and operating parameters on carbon dioxide recovery in polytetrafluoroethylene membranes

Shia-Chung Chen[a,b], Su-Hsia Lin[c,*], Rean-Der Chien[d], Ping-Shun Hsu[a]

[a] Department of Mechanical Engineering, Chung Yuan Christian University, Chung-Li 32023, Taiwan, ROC
[b] R&D Center for Membrane Technology, Chung Yuan University, Chung-Li 32023, Taiwan, ROC
[c] Department of Chemical and Materials Engineering, Nanya Institute of Technology, Chung-Li 32091, Taiwan, ROC
[d] Department of Mechanical Engineering, Nanya Institute of Technology, Chung-Li 32024, Taiwan, ROC

ARTICLE INFO

*Article history:*
Received 30 June 2009
Received in revised form 8 March 2010
Accepted 13 March 2010
Available online 19 March 2010

*Keywords:*
Carbon dioxide absorption
Piperazine
2-Amino-2-methyl-1-propanol
Monoethanolamine
Polytetrafluoroethylene membrane
Asymmetric membrane
Mixed absorbent
Wetting

ABSTRACT

In this study, the recovery of carbon dioxide using an absorbent composed of 2-amino-2-methyl-l-propanol (AMP) + monoethanolamine (MEA) + piperazine (PZ) in polytetrafluoroethylene (PTFE) membrane contactors was investigated. Experiments were conducted using various gas flow rates, liquid flow rates, absorbent blends, and pore size membranes. $CO_2$ recovery increased with increasing liquid flow rates. The blended amine absorbent had a synergistic effect on $CO_2$ recovery. $CO_2$ recovery increased as the pore size of the PTFE membrane decreased. An asymmetric membrane had a better $CO_2$ recovery than that of symmetric membrane. Besides, membrane mass transfer coefficient and operational stability of asymmetric membrane were enhanced. For an asymmetric membrane, the smaller pore-size side of the membrane surface contacting the liquid phase can reduce the level of wetting of the membrane.



## 1. Introduction

Carbon dioxide is the most heavily emitted anthropogenic greenhouse gas, and is believed to be responsible for increases in the earth's surface temperature. Half of all $CO_2$ emissions are from fossil fuel-burning electric power plants [1]. Therefore, the development of a separation processes for removal and recovery of $CO_2$ from these emission sources is greatly needed. In general, bubble columns, packed towers, venturi scrubbers, and/or sieve trays can be used to remove $CO_2$ from process streams. The best-known commercial process for $CO_2$ separation is the packed-column system; however, because of the disadvantages of the packed-column system, which include flooding, channeling, and the need for large-scale equipment, new technologies are needed.

Gas absorption membrane (GAM) processes are an alternative $CO_2$ removal technique. Membrane contactors offer a much larger contact area per unit volume compared to tray and/or packed columns. They have the advantages of no flooding, no entrainment, and no foaming-limited flow rate restrictions [2,3]. However, the additional mass transfer resistances of membranes limit the $CO_2$ absorption rate in the membrane contactor module even though the interfacial area of the membrane is greater than that of conventional absorbers [4]. Therefore, minimization of the membrane mass transfer resistance is an important goal in gas absorption processes that use membrane contactors. The success of GAM technology is highly dependent on the resistance of membrane and wetting of membrane. It is preferable to use hydrophobic membranes for $CO_2$ absorption processes due to the fact that they display fewer wetting and swelling phenomena.

PTFE is considered one of the most suitable materials due to its high hydrophobicity. Yeon et al. [5] investigated $CO_2$ absorption in poly(vinylidene fluoride) (PVDF) and PTFE hollow-fiber membranes using a single absorbent MEA. Kumar et al. [6] studied $CO_2$ capture from dilute gas streams using a novel absorbent called CORAL in a PTFE membrane contactor. Kim and Yang [7] used aqueous alkanolamine solutions as absorbents to separate $CO_2$–$N_2$ mixtures in PTFE hollow fiber membrane contactors. de Montigny et al. [8] used polypropylene and PTFE membranes in a membrane contactor for $CO_2$ absorption. Shimada et al. [9] studied $CO_2$ absorption using AMP with PTFE membrane. However, the broad pore size distribution, membrane thickness and larger pore size of commercial PTFE restrict its application in $CO_2$ absorption. It is difficult to control the pore size of PTFE membranes, though several methods of control have been reported, including heating, plasma

* Corresponding author. Fax: +886 3 4652040.
*E-mail address:* sslin@nanya.edu.tw (S.-H. Lin).

0304-3894/$ – see front matter © 2010 Elsevier B.V. All rights reserved.
doi:10.1016/j.jhazmat.2010.03.057

**Nomenclature**

| | |
|---|---|
| $a$ | gas–liquid contact area ($m^2/m^3$) |
| $D_e$ | average of diffusivity defined by Eq. (9) ($m^2/s$) |
| $D_g$ | diffusivity of $CO_2$ in the gas phase ($m^2/s$) |
| $D_k$ | Knudsen diffusivity of $CO_2$ ($m^2/s$) |
| $D_L$ | diffusivity of $CO_2$ in liquid phase ($m^2/s$) |
| $d_h$ | hydraulic diameter of the module (m) |
| $d_p$ | membrane pore size (μm) |
| $E$ | enhancement factor |
| $H_e$ | Henry's law constant for $CO_2$ ($m^3$ kPa/kmol) |
| $J$ | flux of $CO_2$ (kmol/$m^2$ s) |
| $k_g$ | gas phase mass transfer coefficient (kmol/s $m^2$ kPa) |
| $k_L$ | liquid film mass transfer coefficient (m/s) |
| $K_L$ | overall liquid phase mass transfer coefficient ($s^{-1}$) |
| $k_m$ | membrane mass transfer coefficient (m/s) |
| $t$ | membrane thickness (mm) |
| $L$ | membrane length (m) |
| $P$ | overall pressure (kPa) |
| $P_g$, $P_i$, $P_m$ | $CO_2$ partial pressures in the bulk gas phase, membrane–liquid interface, and gas–membrane interface, respectively (kPa) |
| $P_M$ | log-mean partial pressure of $CO_2$ (kPa) |
| $P_c$ | the critical gas pressure (kPa) |
| $Q_G$ | volumetric flow rate of gas phase stream ($m^3/s$) |
| $Q_L$ | volumetric flow rate of liquid phase stream ($m^3/s$) |
| $R_{CO_2}$ | absorption rate of reaction of $CO_2$ (kmol/$m^3$ s) |
| $R$ | gas constant (kJ/mol K) |
| $R^2$ | correlation coefficient |
| $R_M$, $R_G$, $R_L$ | resistances for membrane, gas-film, and liquid-film diffusion, respectively (s/m) |
| $T$ | absolute temperature (K) |
| $v_g$ | velocity of gas phase (m/s) |
| $v_L$ | velocity of liquid phase (m/s) |

*Greek letters*

| | |
|---|---|
| $\alpha$ | penetration ratio of liquid |
| $\mu_g$ | viscosity of gas (Pa s) |
| $\rho$ | density of gas phase ($kg/m^3$) |
| $\varepsilon$ | membrane porosity |
| $\Delta_M$, $\Delta_G$, $\Delta_L$ | fractional resistances of membrane, gas-film and liquid-film diffusion to overall resistances defied by Eq. (13) |
| $\tau$ | fiber tortuosity |
| [ ] | species concentration ($mol/dm^3$) |

deposition, and sheet/film rolling and stretching [10,11]. The sheet/film rolling and stretch process is most economical method of production. Highly permeable PTFE membranes have been made by this way [10–12]. $CO_2$ recovery of GAM is strongly dependent on the characteristic of membrane, such as pore size, porosity, and thickness of membrane. The influence of those characteristic parameters of membrane on the $CO_2$ recovery is important for its application. To the best of my knowledge, there is few report investigated the difference of $CO_2$ recovery using the various PTFE membranes.

In this study, the different stretching and heating methods was used to manufacture various PTFE membranes including symmetric and asymmetric membranes. $CO_2$ recovery using various membranes in a flat-plate membrane contactor using the aqueous blended alkanolamines solution was investigated. The effects of membrane characteristic, liquid flow rates, gas flow rates, blended absorbents, and wetting on $CO_2$ recovery were examined. Mass transfer resistances were also evaluated.

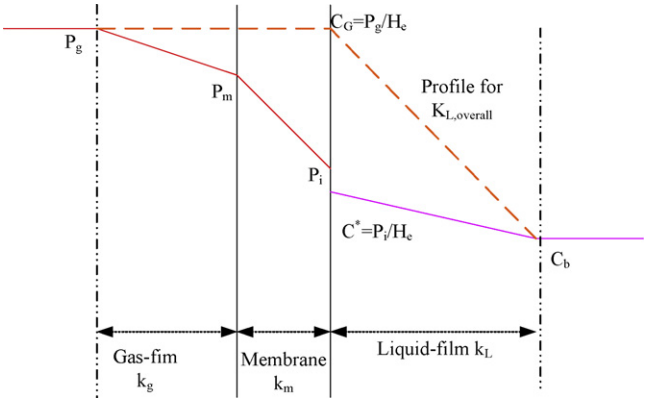


**Fig. 1.** Film model for mass transfer across an ideal non-wetted membrane.

## 2. Theory

### 2.1. Film model

Mass transfer between gas and liquid through a flat-plate membrane contactor occurs in three parts: the gas film, the membrane, and the liquid film shown as Fig. 1 [5]. The $CO_2$ flux per unit length at any cross-section, $J$ (kmol $m^{-2}$ $s^{-1}$), can be expressed by Eq. (1):

$$J = K_L\left(\frac{P_g}{H_e}\right) = k_g(P_g - P_m) = \left(\frac{k_m}{RT}\right)(P_m - P_i) = k_L E\left(\frac{P_i}{H_e}\right) \quad (1)$$

where $k_L$, $k_m$, and $k_g$ are the mass transfer coefficients (m $s^{-1}$) of the liquid phase, membrane, and gas phase, respectively; $K_L$ is an overall liquid phase mass transfer coefficient (m $s^{-1}$); $P_g$, $P_i$, and $P_m$, are the partial pressures (kPa) of $CO_2$ in the bulk gas phase, membrane–liquid interface, and gas–membrane interface, respectively; $H_e$ is Henry's constant for $CO_2$ ($m^3$ kPa $kmol^{-1}$); and $E$ is an enhancement factor for the liquid phase mass transfer coefficient due to chemical reaction [13]. In case of a fast reaction the enhancement factor is given by Eq. (2).

$$E = \frac{(k_r C_b D_L)^{1/2}}{k_L} \quad (2)$$

where $k_r$ is the second-order reaction rate constant ($m^3$ (kmol s)$^{-1}$); $C_b$ is the bulk concentration of active component (kmol $m^{-3}$); $D_L$ is the $CO_2$ diffusion coefficient in liquid phase ($m^2$ $s^{-1}$).

The overall resistance in liquid-phase mass transfer through the flat-plate membrane contactor can be derived by Eq. (1) and expressed by Eq. (3) [14]:

$$\frac{1}{K_L} = \left(\frac{1}{k_g}\right)\left(\frac{1}{H_e}\right) + \left(\frac{1}{k_m}\right)\left(\frac{RT}{H_e}\right) + \left(\frac{1}{Ek_L}\right). \quad (3)$$

If the flows on both sides are assumed as ideal plug-flow, the average driving force on gas phase is log-mean concentration difference of the $CO_2$ solute [5]. The overall mass transfer coefficient, $K_L$, can be obtained by Eq. (4):

$$K_L a = \frac{R_{CO_2}}{(\Delta C)_M} \quad (4)$$

where $R_{CO_2}$ is the $CO_2$ absorption rate per unit volume of the contactor (kmol $m^{-3}$ $s^{-1}$) and $a$ is the gas–liquid contact area ($m^2$ $m^{-3}$). The logarithmic mean concentration difference of $CO_2$, $\Delta C_M$ can be calculated as follows:

$$(\Delta C)_M = \frac{(HC_{g,in} - C_{l,out}) - HC_{g,out}}{In[(HC_{g,in} - C_{l,out})/(HC_{g,out})]} \quad (5)$$

where $C_{g,in}$ and $C_{g,out}$ are the $CO_2$ concentrations at the gas inlet and outlet, respectively. $C_{l,out}$ is the $CO_2$ concentration at liquid outlet.

**Table 1**
Characteristics of various PTFE membranes.

| PTFE | Mean pore size (μm) | Porosity | Thickness (mm) | Stretching frequency | Stretching rate (m/min) | Contact angle ($\theta$) |
|---|---|---|---|---|---|---|
| Symmetric (a) | 0.116 | 0.41 | 0.11 | 1 | 2 | 113.4 |
| Symmetric (b) | 0.29 | 0.52 | 0.17 | 2 | 1 | 118.9 |
| Symmetric (c) | 0.43 | 0.33 | 0.17 | 1 | 2 | 123.4 |
| Symmetric (d) | 0.72 | 0.38 | 0.092 | 1 | 2 | |
| Symmetric (e) | 1.3 | 0.39 | 0.084 | 2 | 2 | |
| Asymmetric (5, 260 °C) (f) | 0.27 | 0.51 | 0.17 | 2 | 1 | 112.9 |
| Asymmetric (5, 300 °C) | 0.25 | 0.51 | 0.17 | 2 | 1 | 114.2 |
| Asymmetric (5, 340 °C) (g) | 0.22 | 0.51 | 0.17 | 2 | 1 | 119.2 |

### 2.2. Individual gas-film mass transfer coefficients

The individual mass transfer coefficient of the liquid phase, $k_L$, can be predicted with Eq. (6) [2,15]:

$$\frac{k_L d_h}{D_L} = 1.62\left(\frac{d_h^2 v_L}{LD_L}\right)^{1/3} \tag{6}$$

where $d_h$ is the hydraulic diameter of the module (m), $v_L$ is the velocity of liquid phase (m s$^{-1}$), and $L$ (m) is the membrane length, and $D_L$ is the diffusivity of $CO_2$ in liquid phase (m$^2$ s$^{-1}$).

The individual mass transfer coefficient of the gas phase has been correlated to Eq. (7) [16]:

$$\frac{k_g d_h}{D_g} = 0.023\left(\frac{d_h \rho v_g}{\mu_g}\right)^{0.8}\left(\frac{\mu_g}{D_g \rho}\right)^{0.33}. \tag{7}$$

where $D_g$ is the diffusivity of $CO_2$ in the gas phase (m$^2$ s$^{-1}$), $v_g$ is the velocity of gas phase (m s$^{-1}$), $\mu_g$ is the viscosity of gas (Pa s), $\rho$ is the density of gas phase (kg m$^{-3}$).

The membrane mass transfer coefficient is predicted using Eq. (8). Here, the effective diffusivity is calculated from the harmonic mean, as shown in Eq. (9).

$$k_m = \frac{D_e \varepsilon}{t\tau} \tag{8}$$

$$\frac{1}{D_e} = \frac{1}{D_k} + \frac{1}{D_g} \tag{9}$$

where $D_e$ is the effective of diffusivity (m$^2$ s$^{-1}$) defined by Eq. (9), $D_k$ is the Knudsen diffusivity of $CO_2$ (m$^2$ s$^{-1}$), $\varepsilon$ is the porosity of the membrane, $\tau$ is the fiber tortuosity and $t$ is the thickness of the membrane (m).

Based on the values for the membrane in Eq. (8), $k_{m,gas\,filled}$ was estimated to be approximately $3.7 \times 10^{-3}$ m s$^{-1}$. In the case of liquid-filled pores, the effective diffusivity is similar to that of $CO_2$ in solution ($1.49 \times 10^{-9}$ m$^2$ s$^{-1}$), and $k_{m,liquid\,filled}$ is about $3.93 \times 10^{-7}$ m s$^{-1}$. If the pores are partially filled with liquid, then $k_m$ can be calculated from the average fractional depth of liquid penetration $\alpha$, as in Eq. (10):

$$\frac{1}{k_m} = \frac{\alpha}{k_{m,liquid\,filled}} + \frac{1-\alpha}{k_{m,gas\,filled}} \tag{10}$$

## 3. Experimental methods

### 3.1. Materials

The PZ, MEA, and AMP were purchased from Aldrich Chemicals Co. The various pore sizes and symmetric and asymmetric PTFE membranes were made by the Research and Development Center for Membrane Technology (CMT). Details of the membranes are listed in Table 1. All chemicals were used without any further purification.

### 3.2. Symmetric PTFE membrane stretching process

The performing and paste extrusion, and stretching processes were described in detail in our previous study [17]. After the PTFE fine powder was extruded into a rod, the rod was rolled in one direction into a sheet with a thickness of 0.2 mm and the lubricant was completely vaporized at 75 °C. Both the extruding and the rolling operations were carried out at room temperature. The major objective is increasing the membrane porous distribution and reducing the pore size. The rolled sheet was stretched uniaxially at different stretching oven temperatures (320 °C) and stretching ratios (50 or 100%). The stretching ratio is defined as:

$$\text{Stretching ratio} = \frac{L_s}{L_o - 1} \times 100\% \tag{11}$$

where $L_s$ is the length of the stretched membrane, $L_o$ is the original length of the sheet before stretched. The stretching frequency of 1 represents that the membrane is stretched with 100% stretching ratio in only one stretching process. However, stretching frequency of 2 represents the membrane achieves with 50% each time in two stretching processes. That is in order to better understand how the stretching ratio affects the membrane morphology under different processing conditions.

### 3.3. Asymmetric heating process

After stretching process, the stretched membrane was treating by asymmetric heating system shown in Fig. 2(a). The heating side (260, 300, 340 °C) at the top of the system and the opposite is the cooling side (5 °C). The membrane passes the asymmetric heating system without stretch in 20 s. The membrane surface facing the heating side was melted and changed its pore size. The membrane surface facing the cooling side maintained their original characteristic including the pore size and pore size distribution. So an asymmetric membrane had two different pore-size membrane surfaces. However a symmetric membrane was the stretched membrane treated in the same temperature on both sides (5, 5 °C) and has the same pore-size membrane surfaces.

### 3.4. Membrane characterization

Surface morphology was analyzed using a field emission SEM (Hitachi S-4800). For the measurement of the mean pore size, a capillary flow porometer (Porous Materials Inc. (PMI, CFP-1500A) was used to analyze the pore size distribution. First, a PTFE membrane sample was cut into a piece 5 cm in diameter and wetted using Porewick1 solution (Porous Materials Inc.). Porewick1 is a standard wetting solution whose surface tension is adjusted to 16 dyne/cm. Then the fully wetted sample is placed in the sample chamber and the chamber is sealed. Gas (nitrogen gas) is then allowed to flow into the chamber behind the sample. When the pressure reaches the point where it overcomes the capillary action of the fluid within the largest pore, the bubble point was found. After determination of the bubble point, the pressure was increased and the flow rate

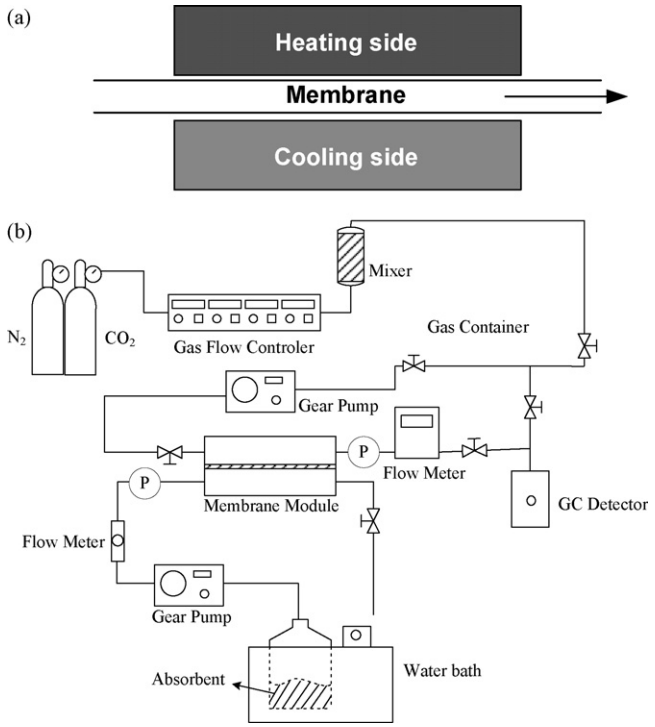


**Fig. 2.** (a) Schematic of stretching operation with asymmetry heating system and (b) experimental set-up.

was measured until all pores were empty and the sample was considered dry. Gas pressure and flow rates through the dry sample were also measured. The pore diameter is calculated according to the following equation [3].

$$d_p = \frac{4\gamma \cos\theta}{P_c} \quad (12)$$

where $d_p$ is the pore diameter, $\gamma$ is the surface tension of the wetting solution, $\theta$ is the contact angle of the wetting solution, and $P_c$ is the critical gas pressure. The $P_c$ is the minimum pressure to be applied on the liquid to enter the pores of the membrane.

### 3.5. Absorption of carbon dioxide

The experimental setup is shown in Fig. 2(b). Gas containing 1–9.5% $CO_2$ (balance $N_2$) was obtained by two mass flow controllers (Brooks Instrument Co., 5850E). The gas was introduced into a packing column (i.d. = 5 cm, length = 30 cm) and mixed completely. The gas was fed into one side of the membrane in the module (wide = 13.7 cm, length = 13.8 cm) until a steady state was reached, then the absorbent was supplied to the other side. All the experiments were conducted in counter-current and one-through operations. Pressure gauges and valves were present to control the flow rates and ensure that a positive pressure of about 14–35 kPa was maintained on the aqueous side of the membranes. The absorbents used in the system consisted of 0.015 mol $dm^{-3}$ PZ, 0.01–0.06 mol $dm^{-3}$ MEA, and 0.01–0.06 mol $dm^{-3}$ AMP. The gas flow rate was varied between 200 and 500 $cm^3$ $min^{-1}$, and the liquid flow rate was varied between 200 and 450 $cm^3$ $min^{-1}$. The gases exiting the absorber were sampled and analyzed with a Thermal Conductivity Detector for Gas Chromatography (GC-14B; Shimadzu) at steady state (ca. 15–20 min). The device can be used for detecting $CO_2$ concentrations ranging from $1 \pm 0.01\%$ to $10 \pm 0.01\%$ $CO_2$ stream. Each experiment was duplicated at least under identical conditions. The reproducibility of the concentration measurements was largely within 5%.

## 4. Results and discussion

### 4.1. Effect of stretching and heating parameters on the characteristic of PTFE membrane

A porous PTFE membrane was formed after the extrudate passes through the rolling and stretching process. From the SEM images shown in Fig. 3, it can be observed that the pore structure of those membranes was fibril-like and the nodes appear regularly in the space along the stretching direction. The pore size and shape of membrane were influenced by the stretching frequency and stretching rate. A smaller stretching rate would make the shape of pore more fibrillar and uniform. The more stretching frequency would lead the nonporous part to become smaller (for example, Fig. 3(b) and (e)) i.e. the more stretching frequency would form a membrane with a higher porosity (Table 1). On the contrary, a larger stretching rate and few stretching frequency formed a less regular pore configuration (Fig. 3(c)) and lower porosity shown in Table 1. The pore size distributions of them were shown in Fig. 4. It can be seen that a larger stretching rate would form a broader pore size distribution as shown in Fig. 4(a), (c), (d), and (e).

The symmetric membrane with the 0.29 μm pore size was chosen to pass the asymmetric heating system at various heating temperature (260, 300, 340 °C). Fig. 5(a) showed the SEM image of the cooling side (5 °C) of membrane surface and Fig. 5(b)–(d) showed the 260, 300, 340 °C-heated membrane surfaces, respectively. It can be seen that the heating process made the membrane surface melt and that resulted in a decrease of the pore size of the membrane surface. The change of pore size distribution by asymmetric heating was also shown in Fig. 4(f) and (g). Comparison with the original one in Fig. 4(b), (f) and (g), we found that the pore size distribution shift to the smaller one. It meant that an increase of the smaller pore sizes on the side of heated membrane surface was found by asymmetric heating process. Such trend was more apparent at a higher heating temperature (340 °C). However it is important to realize the thickness of melted membrane by heating because that the melted thickness affects the resistance of mass transfer in the membrane. A cross-sectional image of the asymmetric membrane (5, 340 °C) was shown in Fig. 6. The bottom of SEM image was the side of the heated membrane (340 °C) and the top one is the side facing cooling system. The white-color part shown in bottom of image in Fig. 6 was the melted part of membrane, which revealed a dense structure. The thickness of melted layer of the membrane seemed much smaller than the non-melted part. For a symmetric membrane (mean pore size 0.29 μm), the mean pore size of the heated side of the membrane was reduced, and was strongly dependent on the heating temperature (260, 300, 340 °C). The mean pore size of the heated side of heated membrane surfaces decreased from 0.27 to 0.22 μm when the heating temperature increased from 260 to 340 °C (Table 1). This is due to the fact that the level of melt was different at different heating temperatures on the membrane surface. Such trend had ever reported in earlier paper [17]. The characteristics of the membrane were influenced by the stretching conditions, such as stretching temperature, stretching rate, stretching direction, and lubricant content [17]. The asymmetric heating process decreased both the pore size and the pore size distribution [17].

### 4.2. Performance comparison of $CO_2$ recovery across various flat membranes

#### 4.2.1. Effect of different blended absorbents on $CO_2$ recovery

Table 2 showed the $CO_2$ recovery ($C/C_0$) using different aqueous blended alkanolamine solutions in a flat-plate PTEF membrane contactor with 0.29 μm symmetric membrane. $C/C_0$ is the $CO_2$ concentration remaining at outlet divided by the initial $CO_2$

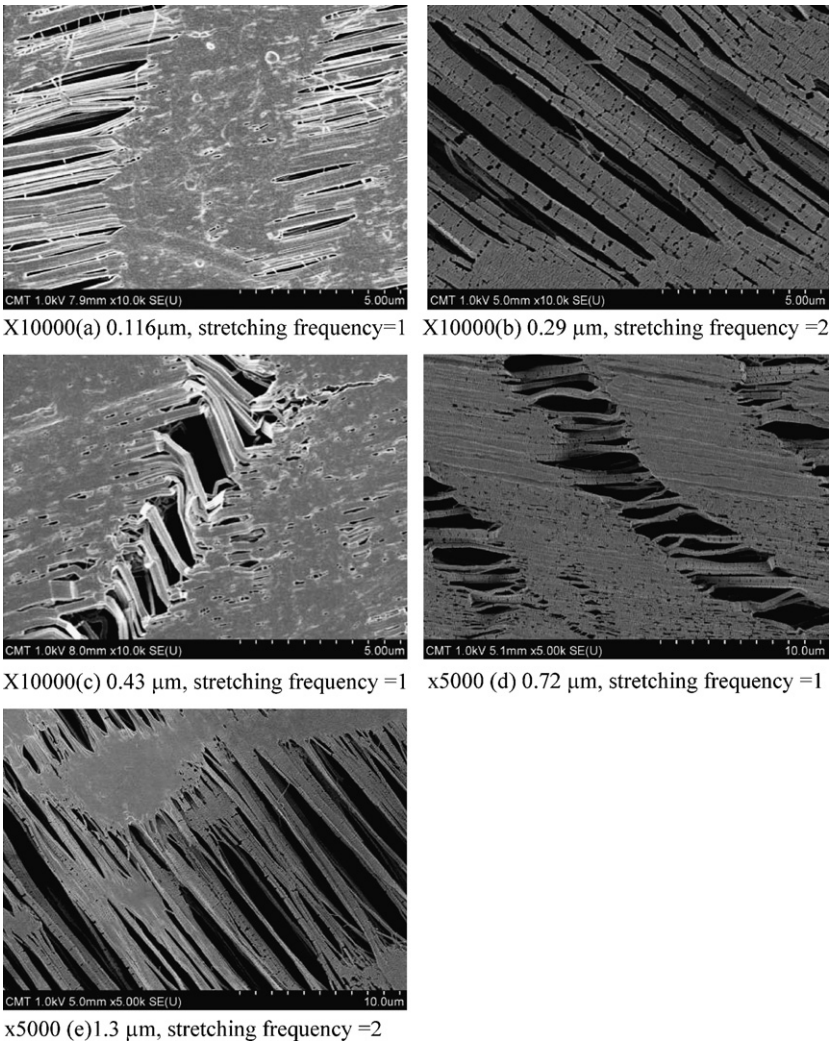


**Fig. 3.** SEM images of various PTFE membranes surface (a) 0.116 μm, (b) 0.29 μm, (c) 0.43 μm, (d) 0.72 μm, and (e) 1.3 μm.

concentration. Table 2 indicated that using an aqueous solution of 0.03 M MEA + 0.03 M AMP + 0.015 M PZ as an absorbent offers the best $CO_2$ recovery. A synergistic effect was found in our system, the phenomenon previously reported in literature [18–22].

*4.2.2. Effect of mean pore size on $CO_2$ recovery*

Fig. 7 showed the $CO_2$ recovery with various mean-pore-sizes symmetric membranes using the 0.03 M MEA + 0.03 M AMP + 0.015 M PZ aqueous solution as an absorbent. We found that $CO_2$ recovery increased with decreasing the mean pore size except the case with the 0.116 μm-membrane. The low $CO_2$ recovery of 0.116 μm-membrane likely resulted from the membrane porosity of 0.116 μm-membrane was lower than that of 0.29 μm-membrane (Table 1). Usually, the wetting of a membrane's pore occurs by the liquid stagnant layer inner the fiber's pores, which depends on the pressure difference of the gas and liquid phases at the membrane's end, namely, critical pressure. This $P_c$ plays an important role in determining the wetting of membrane and the stability of the gas–liquid interface. In general, according to Eq. (12), the larger pore size would lower the critical pressure between the gas and liquid phase. The low critical pressure means an increase of wetting of membrane pore, which work as a kind of membrane resistance. If the operation pressure larger than $P_c$, the breakthrough of membrane will occur. In other words, a higher $P_c$ of the system displays a higher stability of the system. Therefore, it is expected that a pore with smaller diameter would reveal a less wetting with absorbents, which leads a higher $CO_2$ recovery.

**Table 2**
$CO_2$ recovery using different blended amine solutions.

| MEA (M) | AMP (M) | $CO_2$ recovery (%) |
|---|---|---|
| 0.06 | 0.0 | 70 |
| 0.03 | 0.03 | 76 |
| 0.0 | 0.06 | 70 |

*4.2.3. The effect of asymmetric heating on the $CO_2$ recovery*

The effect of asymmetric heating of the membrane on $CO_2$ recovery was shown in Fig. 8. It can be seen that $CO_2$ recovery using an asymmetric membrane (5, 300 °C) was larger than that using a symmetric membrane (5, 5 °C). Further, the $CO_2$ recovery of the membrane contactor using the smaller pore-size side of the membrane facing the gas and liquid phases was also examined as shown in Fig. 8. As Fig. 8 shows, the $CO_2$ recovery of the membrane contactor using the side of heated membrane surface contacting the liquid phase was larger than that facing the gas phase. This is due to the fact that the wetting of membrane with a smaller mean pore size was lower than that with a larger mean pore size. It would be evidenced in Section 4.3.

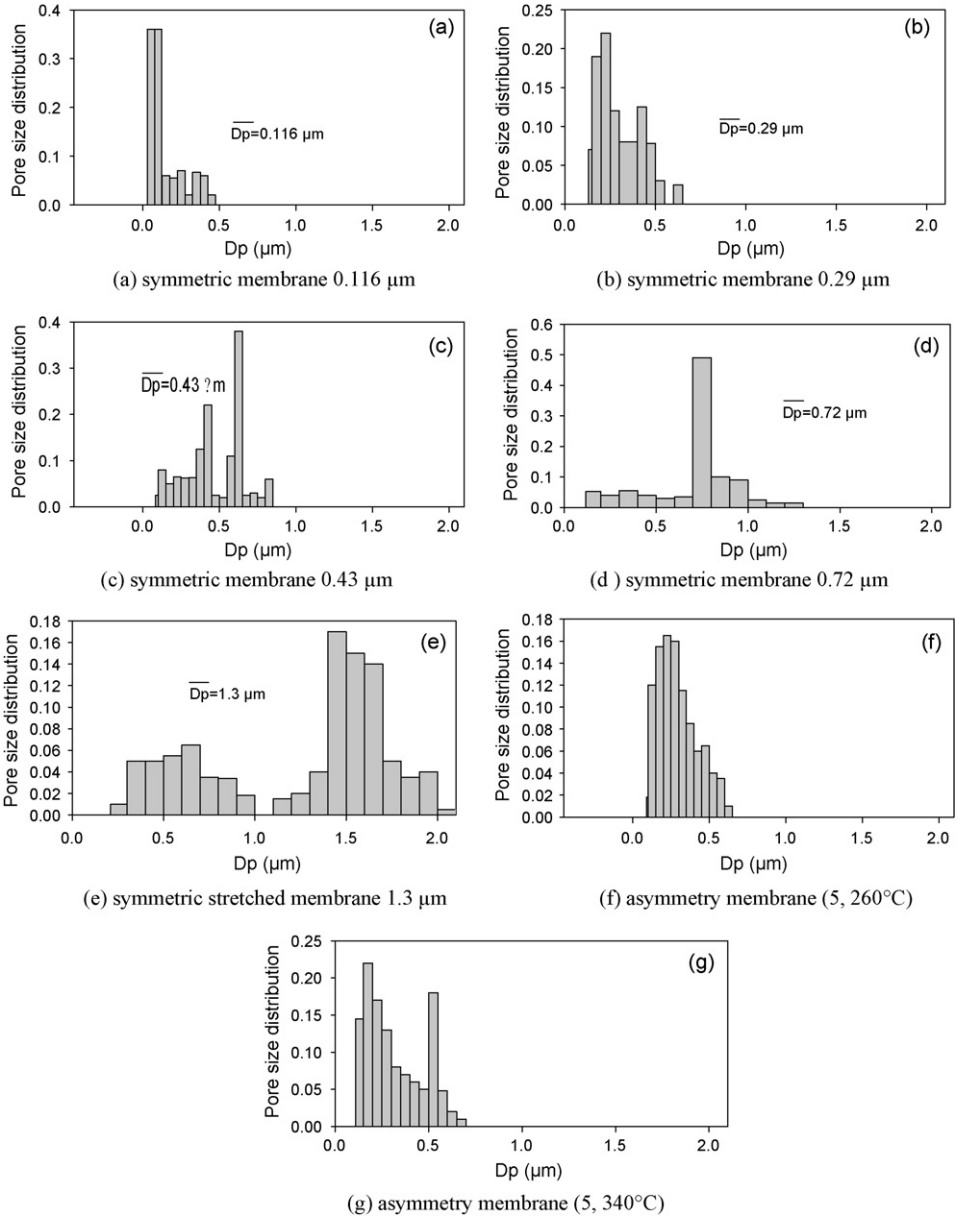


**Fig. 4.** Pore size distribution of various PTFE membranes (a) 0.116 μm, (b) 0.29 μm, (c) 0.43 μm, (d) 0.72 μm, (e) 1.3 μm, (f) asymmetry heating 0.29 μm (5, 260 °C), and (g) asymmetry heating 0.29 μm (5, 340 °C).

#### 4.2.4. *Effect of operating parameters on $CO_2$ recovery*

Figs. 7 and 8 also show the effect of liquid flow rates on $CO_2$ recovery using 0.03 M MEA + 0.03 M AMP + 0.015 M PZ aqueous solution as an absorbent. $CO_2$ recovery appears to increase with increasing liquid flow rate. This increase occurs because that a high velocity in the liquid phase reduces the resistance of the stagnant-layer diffusion under laminar flow. However, $CO_2$ recovery decreases with increasing gas flow rate under the conditions studied (Fig. 9). It is due to fact that the retention time of gas phase in membrane contactor is short at a high gas flow rate. Actually, the $CO_2$ absorption flux increases with increasing gas flow rates (Fig. 9).

### 4.3. *Comparison of wetting ratios for various PTFE membranes*

According to Eq. (4), if we changed various gas flow rate at constant liquid flow rate, the second and third terms in right hand of Eq. (4) would be a constant. As described in our earlier paper [23], the Wilson plot of $1/K_L$ vs. $X = 1/[H_e v_g^{0.83}]$ would be a linear line. Fig. 10 ($R^2 = 0.98$) showed the Wilson plots for symmetric (0.29 μm) and asymmetric (0.25 μm) PTFE membranes contactors with 0.03 M MEA + 0.03 M AMP + 0.015 M PZ solution. The high $R^2$ indicates the correctness of this method. From the intercepts $b$ ($b = 1/Ek_L + 1/k_m(RT/H_e)$) in Fig. 10 (i.e. the value of $1/K_L$ when $X = 0$), we can obtain the measured $k_m$ if $k_L$ was known (calculated by Eq. (6)). Using Eq. (10), the values of the wetting ratio ($\alpha$) are calculated if $k_{m,liquid\,filled}$ and $k_{m,gas\,filled}$ are known (calculated by Eq. (8)) and shown in Table 3. As shown in Table 3, $k_m$ increased with decreasing wetting ratio $\alpha$. A small wetting ratio means that few liquid phase

**Table 3**
Wetting ratio of $\alpha$ and $km$ for various PTFE membranes.

| 0.03 M MEA + 0.03 M AMP + 0.015 M PZ | | |
|---|---|---|
| PTFE membrane | $k_m \times 10^4$ (m/s) | $\alpha \times 10^3$ |
| Symmetric (0.29μm) | 1.5 | 3.72 |
| Asymmetric (0.25 μm) (5, 300 °C) | 3.0 | 0.73 |

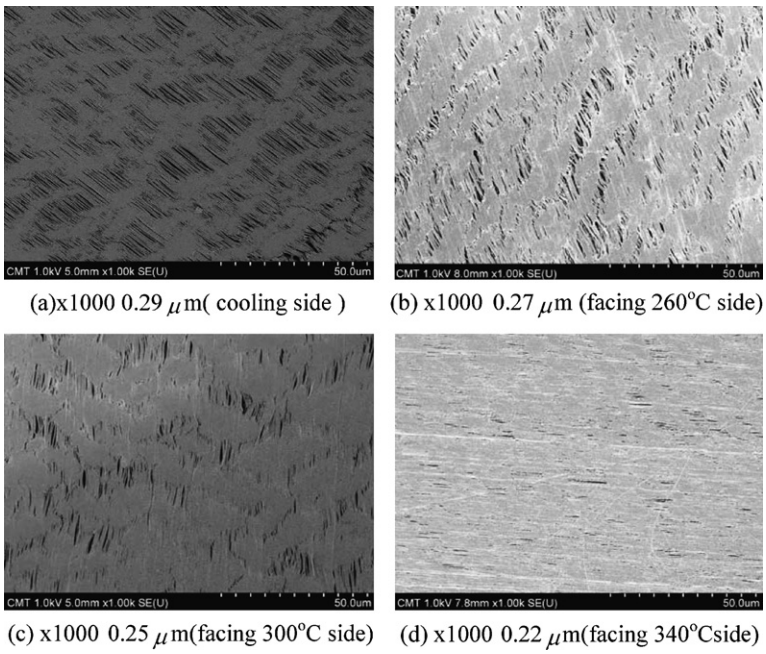


**Fig. 5.** SEM images of symmetric and asymmetric heated membrane surface (a) 0.29 μm (cooling side), (b) 0.27 μm (facing 260 °C side), (c) 0.25 μm (facing 300 °C side), and (d) 0.22 μm (facing 340 °C side).

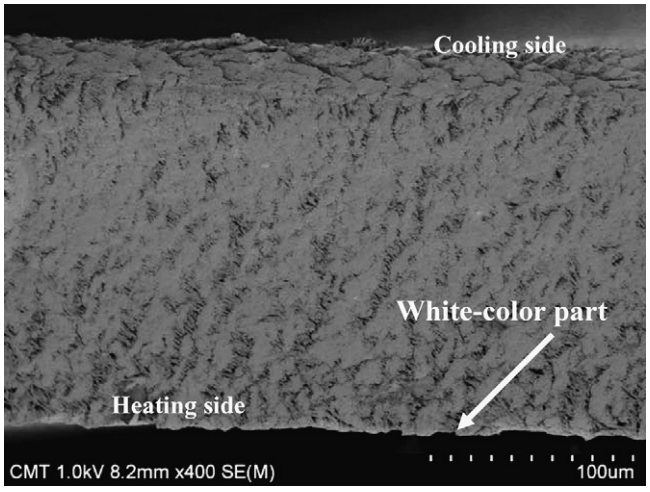


**Fig. 6.** SEM image of cross-section of asymmetric heated membrane (5, 340 °C).

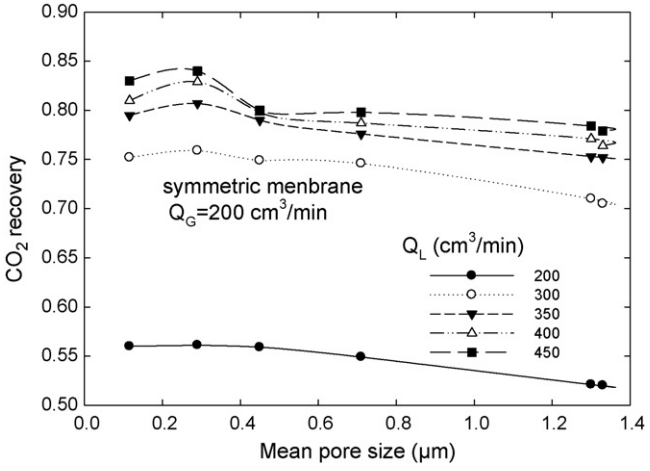


**Fig. 7.** $CO_2$ recovery using various pore-size PTFE membranes with 0.03 M MEA + 0.03 M AMP + 0.015 M PZ solution at $Q_G$ = 200 cm$^3$/min.

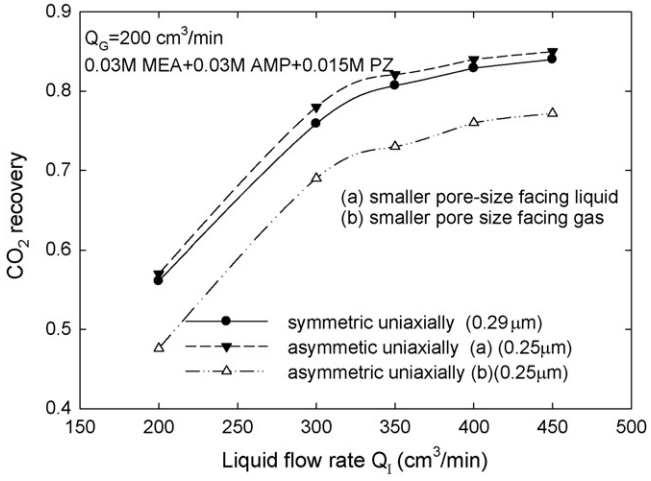


**Fig. 8.** $CO_2$ recovery at various liquid flow rates using different PTFE membranes.

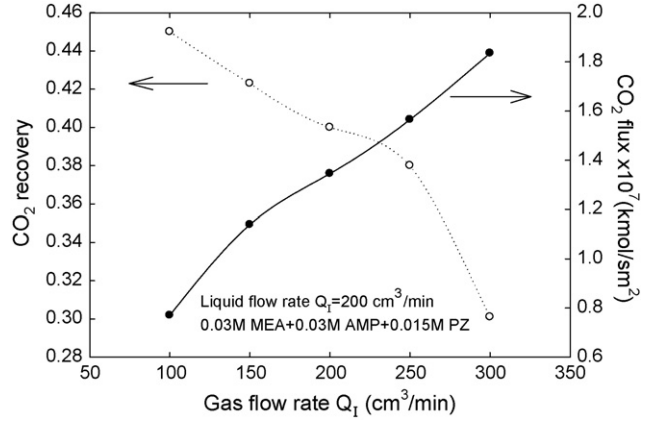


**Fig. 9.** $CO_2$ recovery at various gas flow rates using symmetric PTFE membranes.

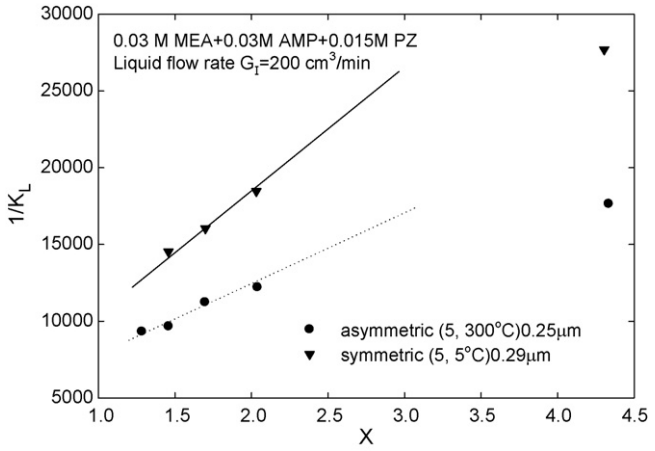


**Fig. 10.** The Wilson-Plot of $1/K_L$ vs. $X$ (0.03 M MEA + 0.03 M AMP + 0.015 M PZ solution, $Q_L$ = 200 cm$^3$/min).

**Table 4**
Fractional resistance of each step in the membrane contactor.

| $Q_G$ (cm$^3$/min) | 100 | 150 | 200 | 250 | 300 |
|---|---|---|---|---|---|
| Asymmetric membrane (5, 300 °C) 0.25 μm | | | | | |
| $\Delta_L$ (%) | 48.1 | 50.7 | 52.3 | 53.7 | 54.7 |
| $\Delta_M$ (%) | 28.0 | 29.5 | 30.6 | 31.3 | 31.9 |
| $\Delta_G$ (%) | 23.8 | 19.7 | 17.0 | 14.9 | 13.4 |
| Symmetric membrane (5, 5°C) 0.29 μm | | | | | |
| $\Delta_L$ (%) | 37.6 | 39.2 | 40.2 | 40.9 | 41.5 |
| $\Delta_M$ (%) | 43.8 | 45.6 | 46.8 | 47.6 | 48.3 |
| $\Delta_G$ (%) | 18.5 | 15.1 | 12.9 | 11.3 | 10.1 |

$Q_L$ = 200 cm/min, $E$ = 20, $H_e$ = 3630 kPa m/kmol.

fills into the membrane pore, which makes a high mass transfer coefficient $k_m$. It is because that the mass transfer rate of $CO_2$ is much higher in gas phase than that in liquid phase. In our case, the smaller pore-size membrane has a lower wetting ratio under identical conditions, which leaded the higher $CO_2$ recovery. So the asymmetric heating is an easily feasible method to enhance the performance of membrane in GAM technology.

### 4.4. Analysis of resistance of mass transfer

To compare the mass transfer resistances in the flat-plate membrane contactor, we express the overall resistance as $1/K_L$, as in Eq. (2). The fractional resistance of each step in the overall process can be calculated, for example, $\Delta_M$ in the hollow fiber module, by Eq. (13):

$$\Delta_M = \frac{R_M}{R_G + R_M + R_L}. \quad (13)$$

$R_M$, $R_G$, and $R_L$ represent the resistances of the membrane, the gas film, and the liquid film, respectively (the terms $(1/k_m)(RT/H_e)$, $(1/k_g)(1/H_e)$, and $1/Ek_L$). The fractional resistances calculated by Eq. (13) for different gas flow rates for asymmetric and symmetric membranes are shown in Table 4. Comparison of these factional resistances shows the rate-controlling steps. In our cases, the gas film resistance never dominates in the ranges studied. The membrane resistance is only important when using a symmetric membrane. Instead, the diffusion resistance of the liquid film always dominated in our systems. The diffusion resistance of the liquid film increased with increasing gas flow rates. Comparison of membrane resistance of those membranes, the membrane resistance of the asymmetric membrane is smaller than that of symmetric membrane. It is due to that the asymmetric membrane has a smaller wetting ratio than the symmetric membrane. The high diffusion resistance in the liquid film was noted by Rangwala [2]. He investigated the $CO_2$ absorption rate using a PP hollow fiber membrane contactor (X-10). In an air–$CO_2$–aq. DEA (0.5 M) system, Rangwala found the fractional resistance of the membrane and the liquid phase to be 20% and 46.2%, respectively.

## 5. Conclusions

Gas absorption processes for removing $CO_2$ in various hydrophobic flat-plate PTFE membrane contactors were investigated. $CO_2$ recovery increases with increasing liquid flow rates. The blended alkanolamines absorbent has a synergistic effect on $CO_2$ recovery (0.03 M MEA + 0.03 M AMP + 0.015 M PZ > 0.06 M MEA + 0.015 M PZ = 0.06 M AMP + 0.015 M PZ). A PTFE membrane formed in a low stretching rate and high stretching frequency would lead a narrow pore size distribution and high membrane porosity. The pore size distribution of membrane would be narrowed by asymmetric heating. The $CO_2$ recovery is enhanced via asymmetric heating treatment. For an asymmetric membrane, the smaller pore-size surface of membrane contacting the liquid phase reduces the level of wetting for the GAM process. The PTFE membrane with asymmetric heating increases not only the membrane mass transfer coefficient but also provided high stability because of its high $P_c$. It is thus feasible to improve the performance of the gas absorption membrane (GAM) via asymmetric heating treatment.

## Acknowledgments

The authors wish to express their sincere gratitude to the Center-of-Excellence (COE) Program on Membrane Technology from the Ministry of Education (MOE), ROC, the project Toward Sustainable Green Technology in the Chung Yuan Christian University, Taiwan, grant CYCU-97-CR-CE, and the National Science and Technology Program - Energy, National Science Council (NSC) for their financial support.

Current research is supported by The Center-of-Excellence Program on Membrane Technology from the Ministry of Education and the project of the specific research fields in the CYCU, Taiwan.

## References

[1] U. Desideri, A. Paolucci, Performance modeling of a carbon dioxide removal system for power plants, Energ. Convers. Manage. 40 (1999) 1899–1915.
[2] H.A. Rangwala, Absorption of carbon dioxide into aqueous solutions using hollow fiber membrane contactors, J. Membr. Sci. 112 (1996) 229–240.
[3] A. Gabelman, S.T. Hwang, Hollow fiber membrane contactors, J. Membr. Sci. 159 (1999) 61–106.
[4] J.L. Li, B.H. Chen, Review of $CO_2$ absorption using chemical solvents in hollow fiber membrane contactors, Sep. Purif. Technol. 41 (2005) 109–122.
[5] S.H. Yeon, B. Sea, Y.I. Park, K.H. Lee, Determination of mass transfer rates in PVDF and PTFE hollow fiber membranes for $CO_2$ absorptions, Sep. Sci. Technol. 38 (2003) 271–293.
[6] P.S. Kumar, J.A. Hogendoorn, P.H.M. Feron, G.F. Versteeg, New absorption liquids for removal of $CO_2$ from dilute gas streams using membrane contactors, Chem. Eng. Sci. 57 (2002) 1639–1651.
[7] Y.S. Kim, S.M. Yang, Absorption of carbon dioxide through hollow fiber membranes using various aqueous absorbents, Sep. Purif. Technol. 21 (2000) 101–109.
[8] D. de Montigny, P. Tontiwachwuthikul, A. Chakma, Using polypropylene and polytetrafluoroethylene membranes in a membrane contactor for $CO_2$ absorption, J. Membr. Sci. 277 (2006) 99–107.
[9] K. Shimada, I.N. Seekkuarachchi, H. Kumazawa, Absorption of $CO_2$ into aqueous solutions of sterically hindered methyl aminoethanol using a hydrophobic microporous hollow fiber contained contactor, Chem. Eng. Commun. 193 (2006) 38–54.
[10] T. Kitamura, K.I. Kurumada, M. Tanigaki, M. Ohshima, S.I. Kanazawa, Formation mechanism of porous structure in polytetrafluoroethylene (PTFE) porous membrane through mechanical operations, Polym. Eng. Sci. 39 (1999) 2256–2263.
[11] T. Kitamura, S. Okabe, M. Tanigaki, K.I. Kurumada, M. Ohshima, S.I. Kanazawa, Morphology change in polytetrafluoroethylene (PTFE), porous membrane caused by heat treatment, Polym. Eng. Sci. 40 (2000) 809–817.
[12] K.I. Kurumada, T. Kitamura, N. Fukumoto, M. Ohshima, M. Tanigaki, S.I. Kanazawa, Structure generation in PTFE porous membranes induced by the uniaxial and biaxial stretching operations, J. Membr. Sci. 149 (1998) 51–57.

[13] M.M. Sharma, P.V. Danckwerts, Absorption of carbon dioxide into solutions of alklis and amines, Chem. Eng. 202 (1966) CE244–CE280.
[14] H. Kreulen, C.A. Smolders, G.F. Versteeg, W.P.M. van Swaaij, Microporous hollow fiber membranes as gas-liquid contactors. Part 2. Mass transfer with chemical reaction, J. Membr. Sci. 78 (1993) 217–238.
[15] E.R. Gilliland, T.K. Sherwood, Diffusion of vapors into air streams, Ind. Eng. Chem. 26 (1934) 516–523.
[16] S. Nii, H. Takeuchi, Removal of $CO_2$ and/or $SO_2$ from gas streams by a membrane absorption method, Gas Sep. Purif. 8 (1994) 107–114.
[17] L.T. Huanga, P.S. Hsua, C.Y. Kuoa, S.C. Chena, J.Y. Lai, Pore size control of PTFE membranes by stretch operation with asymmetric heating system, Desalination 233 (2008) 64–72.
[18] J. Xiao, C.W. Li, M.H. Li, Kinetics of absorption of carbon dioxide into aqueous solutions of 2-amino-2-methyl-1-propanol + monoethanolamine, Chem. Eng. Sci. 55 (2000) 161–175.
[19] W.C. Sun, C.B. Yong, M.H. Li, Kinetics of the absorption of carbon dioxide into mixed aqueous solutions of 2-amino-2-methyl-l-propanol and piperazine, Chem. Eng. Sci. 60 (2005) 503–516.
[20] D.A. Glasscock, J.E. Critchfield, G.T. Rochelle, $CO_2$ absorption/desorption in mixtures of methyldiethanolamine with monoethanolamine or diethanolamine, Chem. Eng. Sci. 46 (1991) 2829–2845.
[21] S.Y. Horng, M.H. Li, Kinetics of absorption of carbon dioxide into aqueous solutions of monoethanolamine + triethanolamine, Ind. Eng. Chem. Res. 41 (2002) 257–266.
[22] H.A. Rangwala, B.R. Morrell, A.E. Mather, F.D. Otto, Absorption of $CO_2$ into aqueous tertiary amine/MEA solutions, Can. J. Chem. Eng. 70 (1992) 482–490.
[23] S.H. Lin, P.C. Chiang, C.F. Hsieh, M.H. Li, K.L. Tung, Absorption of carbon dioxide by the absorbent composed of piperazine and 2-amino-2-methyl-1-propanol in PVDF membrane contactor, J. Chin. Inst. Chem. Eng. 31 (2008) 13–21.